

1 Evidence for rapid weathering response to climatic warming
2 during the Toarcian Oceanic Anoxic Event

3 Theodore R. Them ^{1,2*}, Benjamin C. Gill¹, David Selby³, Darren R. Gröcke³, Richard M.
4 Friedman⁴, and Jeremy D. Owens²

5 ¹*Department of Geosciences, Virginia Polytechnic Institute and State University, Blacksburg,
6 Virginia 24061, USA*

7 ²*Department of Earth, Ocean and Atmospheric Science & National High Magnetic Field
8 Laboratory, Florida State University, Tallahassee, Florida 32306, USA*

9 ³*Department of Earth Sciences, Durham University, Durham, DH1 3LE, UK*

10 ⁴*Pacific Centre for Isotopic and Geochemical Research, Department of Earth, Ocean and
11 Atmospheric Sciences, University of British Columbia, Vancouver, V6T 1Z4, Canada*

12

13 *Email: tthem@fsu.edu

14

15 **Chemical weathering consumes atmospheric carbon dioxide through the breakdown**
16 **of silicate minerals and is thought to stabilize Earth's long-term climate. However, the**
17 **potential influence of silicate weathering on atmospheric $p\text{CO}_2$ levels on geologically short**
18 **timescales ($10^3 - 10^5$ years) remains poorly constrained. Here we focus on the record of a**
19 **transient interval of severe climatic warming across the Toarcian Oceanic Anoxic Event or**
20 **T-OAE from an open ocean sedimentary succession from western North America. Paired**
21 **osmium isotope data and numerical modelling results suggest that weathering rates may**
22 **have increased by 215% and potentially up to 530% compared to the pre-event baseline,**

23 **which would have resulted in the sequestration of significant amounts of atmospheric CO₂.**
24 **This process would have also led to increased delivery of nutrients to the oceans and lakes**
25 **stimulating bioproductivity and leading to the subsequent development of shallow-water**
26 **anoxia, the hallmark of the T-OAE. This enhanced bioproductivity and anoxia would have**
27 **resulted in elevated rates of organic matter burial that would have acted as an additional**
28 **negative feedback on atmospheric pCO₂ levels. Therefore, the enhanced weathering**
29 **modulated by initially increased pCO₂ levels would have operated as both a direct and**
30 **indirect negative feedback to end the T-OAE.**

31 The chemical weathering of rocks constitutes a negative and stabilizing feedback to
32 Earth's long-term (10^8 – 10^9 yr) climate by consuming atmospheric CO₂, modulating the
33 greenhouse effect and, in turn, global temperatures^{1,2,3}. On these timescales, chemical weathering
34 is dominantly regulated by tectonics, atmospheric pCO₂, temperature, the lithology of materials
35 being weathered, and the strength of the hydrological cycle³. Although the influence of
36 weathering on long-term climate is well established³, much less is known about how this process
37 potentially operates and influences climate on shorter times scales ($<10^6$ yr)⁴.

38 The T-OAE of the Early Jurassic Period constituted an ephemeral interval of global
39 warming, perturbations in the global carbon cycle⁵, widespread oceanic anoxia⁶, and elevated
40 marine extinction rates⁷. These environmental and ecological changes have been linked to the
41 emplACEMENT of the Karoo-Ferrar Large Igneous Province (LIP) and subsequent injection of
42 greenhouse gases into the atmosphere⁸ (Fig. 1). Specifically, the addition of mantle-derived CO₂
43 and thermogenic CH₄ derived from the emplacement of the LIP^{9,10,11} and subsequent releases of
44 CH₄ from marine clathrates^{12,13} and terrestrial environments^{14,15} to the oceans and atmosphere are
45 the proposed drivers of the T-OAE warming and carbon cycle perturbations. These perturbations

46 are now recorded in sedimentary successions as pronounced negative carbon isotope excursions
47 (CIEs), which occurred during a long-term trend to more positive carbon isotope values. This
48 negative excursion is followed by a positive CIE thought to be the result of enhanced organic
49 matter burial under anoxic conditions in marine and lacustrine environments^{5,6}. Collectively,
50 these two carbon isotope excursions are used to stratigraphically define the T-OAE interval.

51 Under the enhanced greenhouse effect triggered by elevated levels of atmospheric
52 greenhouse gases during the T-OAE, global temperatures would have increased and the
53 hydrological cycle would have strengthened⁵. Rising $p\text{CO}_2$, global temperatures, and
54 precipitation rates would have led to accelerated weathering rates³. To investigate the proposition
55 of accelerated weathering during the T-OAE, we have utilized osmium isotope ($^{187}\text{Os}/^{188}\text{Os}$)
56 stratigraphy to reconstruct the $^{187}\text{Os}/^{188}\text{Os}$ composition of seawater over the event (see
57 Supplemental Information).

58 The $^{187}\text{Os}/^{188}\text{Os}$ composition of seawater ($^{187}\text{Os}/^{188}\text{Os}_{\text{sw}}$) reflects the sources of osmium to
59 the ocean: rivers that drain continents ($^{187}\text{Os}/^{188}\text{Os}_{\text{cont}} \approx 1.4$) and aeolian dust ($^{187}\text{Os}/^{188}\text{Os}_{\text{aeol}} \approx$
60 1.04) represent a radiogenic end-member, and alteration of juvenile ocean crust or from the
61 mantle ($^{187}\text{Os}/^{188}\text{Os}_{\text{m}} \approx 0.12$) and cosmic dust/bolides ($^{187}\text{Os}/^{188}\text{Os}_{\text{cos}} \approx 0.12$) represent an
62 unradiogenic end-member¹⁶ (SI Fig. 1 and Supplemental Information). The flux of cosmic and
63 aeolian dust represents a small fraction of the global input of osmium to the oceans and does not
64 readily dissolve in seawater, and therefore does not appreciably affect the ocean's $^{187}\text{Os}/^{188}\text{Os}_{\text{sw}}$
65 composition^{16,17}. The present-day $^{187}\text{Os}/^{188}\text{Os}_{\text{sw}}$ (~ 1.06) reflects the relatively greater input of
66 continental-derived osmium to the ocean as compared to mantle-sourced osmium. Importantly,
67 the short residence time of osmium in the oceans ($\sim 10^3\text{-}10^4$ yr)¹⁸ permits the osmium isotope
68 system to record ephemeral changes in global weathering patterns on the order of 10^3 to 10^5

69 years in the geological record¹⁹.

70 The $^{187}\text{Os}/^{188}\text{Os}$ compositions of organic-rich sediments are known to record the
71 $^{187}\text{Os}/^{188}\text{Os}$ composition of contemporaneous seawater¹⁹, and serve as an archive of the past
72 marine osmium isotope compositions. A previous osmium isotope study of the T-OAE interval
73 from a sedimentary succession in the Cleveland Basin of Yorkshire, United Kingdom indicates
74 that, during the event, there was a concomitant, transient increase of $^{187}\text{Os}/^{188}\text{Os}_{\text{sw}}$ values by 0.7²⁰
75 (Fig. 2). This record was originally interpreted to be the result of an increase in continental
76 weathering rates of 400 to 800%²⁰. However, it has been suggested that these data reflect
77 regional climatic changes where enhanced local runoff influenced the $^{187}\text{Os}/^{188}\text{Os}_{\text{sw}}$ composition
78 of the European epicontinental sea, which the Cleveland Basin was part of (Fig. 1), and therefore
79 the $^{187}\text{Os}/^{188}\text{Os}$ record does not reflect a global weathering signal²¹. Key to this dispute is
80 whether the Cleveland Basin was significantly hydrographically restricted so the local
81 $^{187}\text{Os}/^{188}\text{Os}_{\text{sw}}$ signal could be modified^{21,22}. A recently published osmium isotope record across
82 the T-OAE from the Mochras borehole²³, located in nearby Wales, displays a much less
83 pronounced excursion of 0.4 during the T-OAE interval (Fig. 2), which further suggests that
84 geochemical changes recorded in the Cleveland Basin were likely influenced by regional
85 climatic and oceanographic dynamics^{18,24,25}.

86 To resolve whether the transient increases in $^{187}\text{Os}/^{188}\text{Os}$ observed across the T-OAE
87 were indeed a global signal, we have investigated the osmium isotope record from the Lower
88 Jurassic Fernie Formation of the Western Canada Sedimentary Basin located in present-day
89 western Alberta (Fig. 1). This new location was situated on the eastern margin of the ocean of
90 Panthalassa and therefore was located in a different ocean basin from the previously studied
91 Yorkshire and Mochras sites (Figs 1 and 2). Ammonite biostratigraphy and carbon isotope

92 stratigraphy of the Fernie Formation at East Tributary of Bighorn Creek has identified the upper
93 Pliensbachian to middle Toarcian interval and the T-OAE CIEs^{15,26,27,28}. Zircon U-Pb dates from
94 two bentonites located near the base of the section also provide temporal constraint and an age
95 model for the section (Fig. 3; see Methods and Supplementary Data). Importantly, the entire
96 interval of the East Tributary succession contains organic-rich strata (2-8% TOC; Figs 1 and 3)¹⁵,
97 and thus represents an ideal location to reconstruct the global $^{187}\text{Os}/^{188}\text{Os}_{\text{sw}}$ over the T-OAE
98 interval (see Supplemental Information).

99 **Results**

100 **$^{187}\text{Os}/^{188}\text{Os}_i$ record from North America**

101 The high-resolution initial $^{187}\text{Os}/^{188}\text{Os}$ ($^{187}\text{Os}/^{188}\text{Os}_i$) record of the East Tributary
102 succession (see Supplemental Information) displays extremely unradiogenic values ($^{187}\text{Os}/^{188}\text{Os}_i$
103 ≈ 0.25) in the Pliensbachian and Lowest Toarcian, followed by a prominent radiogenic excursion
104 ($^{187}\text{Os}/^{188}\text{Os}_i \approx 0.6$) during the Toarcian CIEs (Fig. 3). The $^{187}\text{Os}/^{188}\text{Os}_i$ values decrease after the
105 Toarcian CIE and asymptotically approach ~ 0.4 (Fig. 3; see Supplemental Information). Locally
106 at East Tributary, aluminum and titanium concentrations increase 3-fold during the $^{187}\text{Os}/^{188}\text{Os}_i$
107 excursion and remain high for the rest of the record (see Fig. 3 and SI Dataset 1), which suggests
108 a local increase in the contribution of continentally derived materials during the event. However,
109 their concentrations remain high as $^{187}\text{Os}/^{188}\text{Os}_i$ values decrease after the Toarcian CIE, which
110 suggests a minimal influence of a detrital component of rhenium and osmium to the osmium
111 isotopic signature (see Fig. 3, Methods, and SI Dataset 1).

112

113 **Discussion**

114 **Comparison of Early Jurassic $^{187}\text{Os}/^{188}\text{Os}_i$ records**

115 Other marine $^{187}\text{Os}/^{188}\text{Os}_i$ records from the Lower Jurassic (Hettangian through Toarcian
116 stages) generally show unradiogenic values^{20,23,29,30}. These are likely related to relatively
117 elevated inputs of unradiogenic osmium from the weathering of the Central Atlantic Magmatic
118 Province (CAMP) and the alteration of juvenile oceanic lithosphere or direct injection of mantle-
119 derived osmium from initial opening of the North Atlantic³¹. The Upper Pliensbachian portion of
120 our record from northeastern Panthalassa has broadly similar values to those observed in the
121 European epicontinental sea^{20,23,29}, which suggests they are representative of the global
122 $^{187}\text{Os}/^{188}\text{Os}_{\text{sw}}$ values, and indicative of a well-mixed Early Jurassic ocean. Further, the East
123 Tributary $^{187}\text{Os}/^{188}\text{Os}_i$ record shows a similar pattern to the other available records during the
124 interval that contains the T-OAE^{20,23}. All the sites record an excursion to higher $^{187}\text{Os}/^{188}\text{Os}_i$
125 values that follow the falling limb of the Toarcian negative CIE. This trend is followed by a
126 return to lower $^{187}\text{Os}/^{188}\text{Os}_i$ values after the rising limb of the negative CIE. However, in all cases
127 $^{187}\text{Os}/^{188}\text{Os}_i$ declines to values slightly higher than those observed before the excursion.

128 While all the $^{187}\text{Os}/^{188}\text{Os}_i$ records display a similar overall pattern, their $^{187}\text{Os}/^{188}\text{Os}_i$
129 values differ. The Yorkshire and East Tributary datasets have similar $^{187}\text{Os}/^{188}\text{Os}_i$ values before
130 and after the T-OAE (~0.3 and ~0.4, respectively); however, the Yorkshire dataset shows an
131 excursion to significantly more radiogenic values ($^{187}\text{Os}/^{188}\text{Os}_i \approx 1$) during the T-OAE²⁰ (Fig. 2).
132 The Mochras data show higher $^{187}\text{Os}/^{188}\text{Os}_i$ values just before the T-OAE CIE (~0.4), which
133 increase to an acme of 0.8 during the T-OAE, and decrease to ~0.3 after the event²³ (Fig. 2).
134 While the absolute $^{187}\text{Os}/^{188}\text{Os}_i$ values differ between the sites, the magnitude of the excursions
135 at East Tributary and Mochras are similar at 0.4, and are almost half the magnitude observed at
136 Yorkshire (0.7).

137 The differences observed between the $^{187}\text{Os}/^{188}\text{Os}_i$ records at East Tributary, Mochras,

138 and Yorkshire suggest there were regional differences in $^{187}\text{Os}/^{188}\text{Os}_{\text{sw}}$ during the studied
139 interval. These differences likely represent local processes such as differing degrees of
140 hydrographic restriction from the open ocean and the amounts of local runoff and its $^{187}\text{Os}/^{188}\text{Os}$
141 composition. However, the similarity in the magnitude of the excursions recorded at East
142 Tributary and Mochras suggest this likely represents the global record of change during the T-
143 OAE. This observation, coupled with the more extreme $^{187}\text{Os}/^{188}\text{Os}_{\text{i}}$ excursion record at
144 Yorkshire, supports the suggestion that the Yorkshire $^{187}\text{Os}/^{188}\text{Os}_{\text{sw}}$ record was influenced by a
145 local riverine input of radiogenic osmium during the T-OAE²¹, and the East Tributary and
146 Mochras records are more representative of global osmium seawater chemistry

147 With these observations in mind, we advocate, when possible, analyzing osmium isotope
148 records from coeval stratigraphic successions deposited in different sedimentary and ocean
149 basins^{18,24,25,26} before attempting to interpret them as a global signal. This methodology is
150 especially important regarding palaeoceanographic studies on intervals older than the Cretaceous
151 since the preserved records are predominantly from continental margin and epicontinental
152 successions, where geochemical signatures have a greater potential to be modified by local
153 processes.

154 **Quantifying the Early Jurassic marine osmium cycle**

155 To gain a more quantitative measure of the changes in the marine osmium cycle during
156 the Toarcian we employed a numerical box model that simulates the osmium inventory of the
157 ocean and its isotopic composition (see Supplemental Information). Specifically, we test whether
158 the osmium isotope excursion associated with the T-OAE (~300 – 500 kyr in duration^{31,32}) can
159 be reproduced by a transient increase in the weathering input of radiogenic osmium to the ocean.
160 We also explored other situations that may have potentially driven the observed T-OAE osmium

161 isotope record, but are likely implausible, such as decreasing the input flux of mantle-derived
162 osmium to zero (see Table 1 for values explored and Supplemental Information for a discussion
163 of these cases). Overall, the numerical model results show that the osmium isotope excursion can
164 be reproduced by a transient three- to six-fold increase in the input of continental-derived
165 osmium to the oceans over 100 to 200 kyr^{31,32} (Fig. 4; more details of the modelling results
166 including sensitivity tests can be found in the Supplemental Information).

167 Changes in the $^{187}\text{Os}/^{188}\text{Os}_{\text{cont}}$ to more radiogenic values through the differential
168 weathering of lithologies such as shales and cratonic rocks^{33,34,35} could have played a role in the
169 T-OAE osmium isotope record. We investigated the potential effect this change would have on
170 the osmium budget during the event by running simulations where we elevated $^{187}\text{Os}/^{188}\text{Os}_{\text{cont}}$
171 from 1.4 to 2 (see Supplemental Information for a discussion of the choice of the maximum
172 $^{187}\text{Os}/^{188}\text{Os}_{\text{cont}}$ value). In these simulations, a nearly three-fold increase of the input of
173 continental-derived osmium to the oceans was still necessary to reproduce the excursion (Fig. 4),
174 regardless of timescale used, and solely increasing $^{187}\text{Os}/^{188}\text{Os}_{\text{cont}}$ to reasonable values cannot
175 reproduce the observed excursion (see Supplemental Information). Given the plausible
176 proposition of the changing composition of the continental weathering flux, we conservatively
177 suggest that T-OAE weathering rates increased by as much as three-fold.

178 A potential source of radiogenic, continental derived osmium was the remnants of the
179 Central Pangaean Mountains, a Himalayan-scale mountain belt in eastern North America and
180 northwestern Africa. This mountain belt was positioned at tropical and subtropical latitudes in
181 the Early Jurassic (Fig. 1). The rifting of Pangaea during the Late Triassic and Early Jurassic
182 would have exposed the core of the mountain range leaving this material open to weathering or
183 erosion. General circulation models predict large increases in the air temperature and runoff

184 during the T-OAE in the geographic region that contained these mountains³⁶. These regional
185 climatic changes would have facilitated enhanced chemical weathering, and makes this mountain
186 belt a plausible source of the enhanced input of osmium to the oceans advocated here.

187 The weathering of organic-rich rocks and sediments would be another plausible way to
188 raise the isotopic composition of the continental weathering flux, but also results in a net release
189 of CO₂ to the atmosphere³⁷. However, enhanced continental runoff would also have increased
190 nutrient delivery and stimulated primary productivity in aquatic environments leading to
191 increased hypoxia, anoxia, and potentially euxinia⁵. Elevated burial of organic matter in these
192 environments would have sequestered much more atmospheric CO₂ than that associated with any
193 black shale weathering, which we suggest represent only a fraction of the continental materials
194 that were predominantly weathered during the event.

195 **Differences in the osmium isotope response between OAE events**

196 A striking feature of the ¹⁸⁷Os/¹⁸⁸Os records during the Mesozoic OAEs is the
197 directionality of their excursions. The T-OAE records show a positive ¹⁸⁷Os/¹⁸⁸Os excursion,
198 whereas the onset of the Cretaceous OAE 1a and OAE 2 both display negative excursions. The
199 difference in the ¹⁸⁷Os/¹⁸⁸Os response to these events most likely lies in the environment where
200 the LIPs were emplaced. The Cretaceous events are associated with subaqueous emplacements
201 of the Ontong Java Plateau (OAE 1a) and the Caribbean and High Arctic LIPs (OAE 2).
202 Emplacement of these LIPs would have supplied large amounts of unradiogenic, mantle-derived
203 osmium directly into the oceans from weathering of basalts on the seafloor, resulting in osmium
204 isotope excursions to nonradiogenic values^{25,38,39,40}.

205 The T-OAE, on the other hand, is associated with a subaerial emplacement of the Karoo-
206 Ferrar LIP at high latitudes (Fig. 1), where the semi-arid climate would have made the relative

207 weathering potential of this material low. In contrast to the younger OAEs, the Toarcian
208 $^{187}\text{Os}/^{188}\text{Os}_i$ records reflect enhancement of the weathering of continental materials facilitated by
209 the injection of greenhouse gases into the atmosphere and subsequent climate changes. Notably,
210 delivery of osmium from the Karoo-Ferrar LIP would have also been delayed, as compared to
211 the Cretaceous LIPs. However, if weathering of the Karoo-Ferrar LIP was a significant source of
212 osmium to the oceans during the T-OAE, then its lower $^{187}\text{Os}/^{188}\text{Os}$ compositions^{41,42,43,44,45}
213 would necessitate an even greater contribution of continental material to generate the observed
214 $^{187}\text{Os}/^{188}\text{Os}_i$ excursion.

215

216 **Implications and Conclusions**

217 Based on the osmium isotope records and our modelling results, the transient increase in
218 continental weathering rates during the T-OAE may be one of the largest observed during the
219 Phanerozoic. Chemical weathering rates are also suggested to have significantly increased across
220 the Permian-Triassic boundary⁴⁶, Triassic-Jurassic boundary^{47,48}, and the Paleocene-Eocene
221 Thermal Maximum⁴⁹, all of which are associated with intervals of global warming,
222 environmental deterioration, and extinction events⁵⁰. The rapid response of the osmium isotope
223 system during the T-OAE, as well as during other OAEs^{38,39,40}, indicates that chemical
224 weathering feedbacks may respond to episodes of rapid climatic warming on short timescales
225 ($10^3 - 10^6$ years) and lead to a net drawdown of atmospheric CO_2 ⁵. Enhanced continental runoff
226 would also have increased nutrient delivery and stimulated primary productivity in nearshore
227 environments, leading to increased marine hypoxia, anoxia, and potentially euxinia⁵. CO_2 would
228 also have been sequestered through the deposition of organic-rich sediments in marine and
229 lacustrine settings^{5,6,51}.

230 In the case of the Toarcian OAE, increased weathering likely played a critical role in
231 reversing the enhanced greenhouse state induced by Karoo-Ferrar magmatism. As atmospheric
232 CO₂ was consumed through these mechanisms, global temperatures would have declined^{5,20}. As
233 modern atmospheric CO₂ levels continue to increase at rates much higher than any point during
234 the Cenozoic⁵², increased weathering, through the chemical and physical weathering feedbacks
235 and stimulation of primary production and subsequent organic matter burial, may eventually act
236 as a negative feedback to global warming, although on timescales much longer than what is
237 necessary to mitigate the immediate environmental and ecological deterioration due to this
238 warming⁵³.

239

240 **Methods**

241 **$\delta^{13}\text{C}$ and total organic carbon analysis**

242 $\delta^{13}\text{C}$ and total organic carbon (TOC) were measured from each sample for rhenium,
243 osmium, and trace metals (see below). The samples were prepared and analysed using the same
244 methods from ref 15.

245

246 **Rhenium and osmium isotopic analysis**

247 In order to isolate primarily the hydrogenous rhenium and osmium from our samples, and
248 minimize the removal of detrital rhenium and osmium, we followed the procedures of ref 54.
249 Between ~0.25 and 1 g of sample powder (dependent upon previously measured rhenium
250 abundances via inductively-coupled plasma mass spectrometry) were digested with a known
251 amount of ¹⁸⁵Re and ¹⁹⁰Os tracer (spike) solutions in 8 mL of a CrO₃-H₂SO₄ solution; this
252 reaction occurred in sealed Carius tubes, which were heated incrementally to 220 °C for 48

253 hours. The tubes were allowed to cool before opening. The osmium was immediately isolated
254 and purified from the acid medium by solvent extraction using chloroform. This step was
255 followed by the back reduction of Os from the chloroform into HBr. The Os fraction was further
256 purified by micro-distillation. Rhenium was purified from the remaining CrO₃-H₂SO₄ solution by
257 a NaOH-Acetone solvent extraction⁵⁵ and further purified using anion exchange
258 chromatography. The purified Re and Os fractions were then loaded onto Ni and Pt filaments,
259 respectively, and analysed for their isotopic composition using negative thermal-ionization mass
260 spectrometry (NTIMS)^{56,57} using a Thermo Scientific TRITON mass spectrometer with static
261 Faraday collection for Re and ion-counting using a secondary electron multiplier in peak-
262 hopping mode for Os. In-house Re and Os solutions were continuously analysed during the
263 course of this study to ensure and monitor long-term mass spectrometry reproducibility. A 125
264 pg aliquot of the Re std solution and a 50 pg aliquot of DROsS yield ¹⁸⁵Re/¹⁸⁷Re values of
265 0.5983 ± 0.002 (1 SD, n = 6) and ¹⁸⁷Os/¹⁸⁸Os values of 0.16089 ± 0.0005 (1SD, n = 8),
266 respectively; both are identical to previously reported values⁵⁷. The measured difference in
267 ¹⁸⁵Re/¹⁸⁷Re values for the Re std solution and the accepted ¹⁸⁵Re/¹⁸⁷Re value (0.5974)⁵⁸ is used
268 for mass fractionation correction of the Re sample data. All Re and Os data are oxide and blank
269 corrected. Procedural blanks for Re and Os in this study were 12 ± 3 pg/g and 0.07 ± 0.05 pg/g,
270 respectively, with an ¹⁸⁷Os/¹⁸⁸Os value of 0.25 ± 0.15 (n = 4). The ¹⁸⁷Re/¹⁸⁸Os and ¹⁸⁷Os/¹⁸⁸Os
271 uncertainties are determined through full propagation of uncertainties, including those in
272 weighing, mass spectrometer measurements, spike calibrations, blank abundances and
273 reproducibility of standard values.

274

275 **Trace metal analysis**

276 In order to compare the changes in [Re] and [Os] to sedimentation patterns across the T-
277 OAE, we also analysed the concentrations of aluminum and titanium in each sample, which are
278 used to estimate the contribution of terrigenous input to a sedimentary basin^{59,60} (see Fig. 3 and
279 SI dataset). Approximately 0.05g of powder was added to a teflon beaker, followed by the
280 addition of 4 mL of a 50:50 mixture of concentrated HCl and concentrated HNO₃. This solution
281 was placed inside a (CEM MARS 5) microwave assisted digestion system and run until all
282 organic material had broken down at a temperature of 150°C. The samples were then dried down
283 and the silicates were dissolved using 4:1 HNO₃ to HF, dried down, and re-dissolved in 5%
284 HNO₃ solution. A 100µL solution split was spiked with an internal standard to measure
285 elemental abundances using an Agilent 7500cs inductively coupled plasma mass spectrometer in
286 He and H mode. Internal standard was used to correct the samples for machine drift.
287 International standards USGS SCO-1 and SDO-1 were also measured and had a reproducibility
288 of $\pm 5\%$.

289

290 **U-Pb analysis of zircons**

291 CA-TIMS procedures described here are modified from refs 61, 62, 63. After rock
292 samples have undergone standard mineral separation procedures zircons are handpicked in
293 alcohol. The clearest, crack- and inclusion-free grains are selected, photographed, and then
294 annealed in quartz glass crucibles at 900°C for 60 hours. Annealed grains are transferred into 3.5
295 mL PFA screwtop beakers, ultrapure HF (up to 50% strength, 500 µL) and HNO₃ (up to 14 N, 50
296 µL) are added and caps are closed finger tight. The beakers are placed in 125 mL PTFE liners
297 (up to four per liner) and about 2 mL HF and 0.2 mL HNO₃ of the same strength as acid within
298 beakers containing samples are added to the liners. The liners are then slid into stainless steel

299 Parr™ high pressure dissolution devices, which are sealed and brought up to a maximum of
300 200°C for 8-16 hours (typically 175°C for 12 hours). Beakers are removed from liners and zircon
301 is separated from leachate. Zircons are rinsed with >18 MΩ.cm water and subboiled acetone.
302 Then 2 mL of subboiled 6N HCl is added and beakers are set on a hotplate at 80°-130°C for 30
303 minutes and again rinsed with water and acetone. Masses are estimated from the dimensions
304 (volumes) of grains. Single grains are transferred into clean 300 µL PFA microcapsules
305 (crucibles), and 50 µL 50% HF and 5 µL 14N HNO₃ are added. Each is spiked with a ²³³⁻²³⁵U-
306 ²⁰⁵Pb tracer solution (EARTHTIME ET535), capped, and again placed in a Parr liner (8-15
307 microcapsules per liner). HF and nitric acids in a 10:1 ratio, respectively, are added to the liner,
308 which is then placed in a Parr high pressure device and dissolution is achieved at 220°C for 40
309 hours. The resulting solutions are dried on a hotplate at 130°C, 50 µL 6N HCl is added to
310 microcapsules and fluorides are dissolved in high-pressure Parr devices for 12 hours at 180°C.
311 HCl solutions are transferred into clean 7 mL PFA beakers and dried with 2 µL of 0.5N H₃PO₄.
312 Samples are loaded onto degassed, zone-refined Re filaments in 2 µL of silicic acid emitter⁶⁴.

313 Isotopic ratios are measured with a modified single collector 354S (with Sector 54
314 electronics) thermal ionization mass spectrometer equipped with analogue Daly photomultipliers.
315 Analytical blanks are 0.2 pg for U and up to 1.9 pg for Pb. U fractionation was determined
316 directly on individual runs using the EARTHTIME ET535 mixed ²³³⁻²³⁵U-²⁰⁵Pb isotopic tracer
317 and Pb isotopic ratios were corrected for fractionation of 0.25 ± 0.03%/amu, based on replicate
318 analyses of NBS-982 reference material and the values recommended by ref. 65. Data reduction
319 employed the excel-based program of ref. 66. Standard concordia diagrams were constructed and
320 regression intercepts, weighted averages calculated with Isoplot⁶⁷. Unless otherwise noted all
321 errors are quoted at the 2-sigma or 95% level of confidence. Isotopic dates are calculated with

322 the decay constants $\lambda_{238}=1.55125\text{E-}10$ and $\lambda_{235}=9.8485\text{E-}10$ (ref. 68) and a $^{238}\text{U}/^{235}\text{U}$ ratio of
323 137.88. EARTHTIME U-Pb synthetic solutions are analysed on an on-going basis to monitor the
324 accuracy of results.

325 Five single zircon grains from the bentonite at -1.9 meters in the East Tributary section
326 (see Fig. 3) were analysed by the uranium-lead chemical abrasion isotope dilution thermal
327 ionization mass spectrometry technique (U-Pb CA-ID-TIMS). A weighted mean $^{206}\text{Pb}/^{238}\text{U}$ age
328 of 188.58 ± 0.17 (0.25) [0.32] Ma, (MSWD=0.89) is based on concordant and overlapping
329 results for three of the analysed grains (see SI Dataset 2). Older results for the other two grains
330 suggest that they are xenocrysts and/or contain inherited cores. It is important to note that this
331 bentonite has a previously published multigrain U-Pb ID-TIMS age of $188.3 +1.5/-1$ Ma⁶⁹.

332 Five single zircon grains from the bentonite at 2.35 meters in the East Tributary section
333 (see Fig. 3) were analysed by the U-Pb CA-ID-TIMS technique. A weighted mean $^{206}\text{Pb}/^{238}\text{U}$
334 age of 185.49 ± 0.16 (0.25) [0.32] Ma, (MSWD=1.17) is based on concordant and overlapping
335 results for three of the analysed grains (see SI Dataset 3). Older results for the other two grains,
336 one of which is discordant, suggest that they are xenocrysts and/or contain inherited cores.

337

338 **Age model and calculation of $^{187}\text{Os}/^{188}\text{Os}_i$**

339 The age model (see below) is constructed using a single grain U-Pb CA-ID-TIMS age of
340 188.58 ± 0.17 (0.25) [0.32] Ma from approximately two meters below the lowest interval with
341 carbon isotope data in the East Tributary section¹⁵ and a single grain U-Pb CA-ID-TIMS age of
342 185.49 ± 0.16 (0.25) [0.32] Ma (see above) located at 2.35 meters in the section (see Fig. 3).
343 Linear interpolation was used to calculate ages between the bentonites layers and between the
344 age assigned for the Toarcian CIE. The onset of the CIE is placed at 183.1 Ma, with a total

345 duration of 300 kyr³¹. Sedimentation rates are also assumed to remain constant after the Toarcian
346 CIE. The initial osmium isotopic composition of the oceans (¹⁸⁷Os/¹⁸⁸Os_i) was calculated using
347 the following equation and the ¹⁸⁷Re decay constant from ref. 70:

348
$$\frac{^{187}\text{Os}}{^{188}\text{Os}_i} = \frac{^{187}\text{Os}}{^{188}\text{Os}} - \left(\frac{^{187}\text{Re}}{^{188}\text{Os}} \times \left(e^{(1.666 \times 10^{-11} \cdot a^{-1} \times \text{age} \times 1000000)} - 1 \right) \right) \quad (1)$$

349 This equation accounts for the ¹⁸⁷Os produced after deposition by the decay of ¹⁸⁷Re. As stated
350 above, the age component was derived from U-Pb ages from this succession (this study) and
351 previously published dates for the age and estimated duration of the Toarcian CIE³¹.
352 Furthermore, if a longer 500-kyr duration³² is assigned to the T-OAE CIE, the calculated
353 ¹⁸⁷Os/¹⁸⁸Os_i values do not change significantly and our interpretations do not change (see
354 Supplemental Information).

355

356 **REFERENCES CITED**

357 1. Walker, J.C.G., Hays, P.B. & Kasting, J.F. A negative feedback mechanism for the long-term
358 stabilization of Earth's surface temperature. *J. Geophys. Res.* **86**, 9776–9782 (1981).

359 2. Berner, R.A., Lasaga, A.C. & Garrels, R.M. The carbonate-silicate geochemical cycle and its
360 effect on atmospheric carbon dioxide over the past 100 million years. *Am. J. Sci.* **283**, 641–
361 683 (1983).

362 3. Kump, L.R., Brantley, S.L. & Arthur, M.A. Chemical Weathering, Atmospheric CO₂, and
363 Climate. *Ann. Rev. Earth Plan. Sci.* **28**, 611–667 (2000).

364 4. Foster, G.L. & Vance, D. Negligible glacial-interglacial variation in continental weathering
365 rates. *Nature* **444**, 918–921 (2006).

366 5. Jenkyns, H.C. Geochemistry of oceanic anoxic events. *G³* **11**, Q03004 (2010).

367 6. Jenkyns, H.C. The Early Toarcian (Jurassic) Anoxic Event: Stratigraphic, Sedimentary, and

368 Geochemical Evidence. *Am. J. Sci.* **288**, 101–151 (1988).

369 7. Harries, P.J. & Little, C.T.S. The early Toarcian (Early Jurassic) and the Cenomanian-
370 Turonian (Late Cretaceous) mass extinctions: similarities and contrasts. *Palaeogeogr.*
371 *Palaeoclim. Palaeoecol.* **154**, 39–66 (1999).

372 8. Pálfy, J. & Smith P.L. Synchrony between Early Jurassic extinction, oceanic anoxic event, and
373 the Karoo-Ferrar flood basalt volcanism. *Geology* **28**, 747–750 (2000).

374 9. McElwain J.C., Wade-Murphy J. & Hesselbo S.P. Changes in carbon dioxide during an
375 oceanic anoxic event linked to intrusion into Gondwana coals. *Nature* **435**, 479–482 (2005).

376 10. Beerling, D.J. & Brentnall S.J. Numerical evaluation of mechanisms driving Early Jurassic
377 changes in global carbon cycling. *Geology* **35**, 247–250 (2007).

378 11. Svensen, H. *et al.* Hydrothermal venting of greenhouse gases triggering Early Jurassic global
379 warming. *Earth Plan. Sci. Lett.* **256**, 554–566 (2007).

380 12. Hesselbo, S.P. *et al.* Massive dissociation of gas hydrate during a Jurassic oceanic anoxic
381 event. *Nature* **406**, 392–395 (2000).

382 13. Kemp, D.B., Coe A.L., Cohen A.S. & Schwark L. Astronomical pacing of methane release in
383 the Early Jurassic period. *Nature* **437**, 396–399 (2005).

384 14. Pieńkowski, G., Hodbod, M. & Ullmann, C.V. Fungal decomposition of terrestrial organic
385 matter accelerated Early Jurassic climate warming. *Scientific Rep.* **6:31030** (2016).

386 15. Them, T.R. II *et al.* High-resolution carbon isotope records of the Toarcian Oceanic Anoxic
387 Event (Early Jurassic) from North America and implications for the global drivers of the
388 Toarcian carbon cycle. *Earth Plan. Sci. Lett.* **459**, 118–126 (2017).

389 16. Peucker-Ehrenbrink, B. & Ravizza, G. The marine osmium isotope record. *Terra Nova* **12**,
390 205–219 (2000).

391 17. Peucker-Ehrenbrink, B. Accretion of extraterrestrial matter during the last 80 million years
392 and its effect on the marine osmium isotope record. *Geochim. Cosmochim. Acta* **60**, 3187–
393 3196 (1996).

394 18. Rooney, A.D. *et al.* Tracking millennial-scale Holocene glacial advance and retreat using
395 osmium isotopes: Insights from the Greenland ice sheet. *Quat. Sci. Rev.* **138**, 49–61 (2016).

396 19. Cohen, A.S., Coe, A.L., Bartlett, J.M. & Hawkesworth, C.J. Precise Re—Os ages of organic-
397 rich mudrocks and the Os isotope composition of Jurassic seawater. *Earth Plan. Sci. Lett.*
398 **167**, 159–173 (1999).

399 20. Cohen, A.S., Coe, A.L., Harding, S.M. & Schwark, L. Osmium isotope evidence for the
400 regulation of atmospheric CO₂ by continental weathering. *Geology* **32**, 157–160 (2004).

401 21. McArthur, J.M., Algeo, T.J., van de Schootbrugge, B., Li, Q. & Howarth, R.J. Basinal
402 restriction, black shales, Re-Os dating, and the Early Toarcian (Jurassic) oceanic anoxic
403 event. *Paleoceanography* **23**, PA4217 (2008).

404 22. Waltham, D. & Gröcke, D.R. Non-uniqueness and interpretation of the seawater ⁸⁷Sr/⁸⁶Sr
405 curve. *Geochim. Cosmochim. Acta* **70**, 384–394 (2006).

406 23. Percival, L.M.E. *et al.* Osmium isotope evidence for two pulses of increased continental
407 weathering linked to Early Jurassic volcanism and climate change. *Geology* **44**, 759–762
408 (2016).

409 24. Paquay, F.S. & Ravizza, G. Heterogeneous seawater ¹⁸⁷Os/¹⁸⁸Os during the Late Pleistocene
410 glaciations. *Earth Plan. Sci. Lett.* **349-350**, 126–138 (2012).

411 25. Du Vivier, A.D.C. *et al.* Marine ¹⁸⁷Os/¹⁸⁸Os isotope stratigraphy reveals the interaction of
412 volcanism and ocean circulation during Oceanic Anoxic Event 2. *Earth Plan. Sci. Lett.* **389**,
413 23–33 (2014).

414 26. Hall, R.L. Lithostratigraphy and biostratigraphy of the Fernie Formation (Jurassic) in the
415 southern Canadian Rocky Mountains, *in* Stott, D.F. & Glass, D.J., eds., The Mesozoic of
416 Middle North America. *Can. Soc. Petr. Geol. Mem.* **9**, 233–247 (1984).

417 27. Hall, R.L. New Lower Jurassic ammonite faunas from the Fernie Formation, southern
418 Canadian Rocky Mountains. *Can. J. Earth Sci.* **24**, 1688–1704 (1987).

419 28. Asgar-Deen, M., Hall, R., Craig, J. & Riediger, C. New biostratigraphic data from the Lower
420 Jurassic Fernie Formation in the subsurface of west-central Alberta and their stratigraphic
421 implications. *Can. J. Earth Sci.* **40**, 45–63 (2003).

422 29. Porter, S.J., Selby, D., Suzuki, K. & Gröcke, D. Opening of a trans-Pangaean marine corridor
423 during the Early Jurassic: Insights from osmium isotopes across the Sinemurian-
424 Pliensbachian GSSP, Robin Hood's Bay, UK. *Palaeogeogr. Palaeoclim. Palaeoecol.* **375**, 50–
425 58 (2013).

426 30. Cohen, A.S. & Coe, A.L., New geochemical evidence for the onset of volcanism in the
427 Central Atlantic magmatic province and environmental change at the Triassic-Jurassic
428 boundary. *Geology* **30**, 267–270 (2002).

429 31. Sell, B. *et al.* Evaluating the temporal link between the Karoo LIP and climatic—biologic
430 events of the Toarcian Stage with high-precision U-Pb geochronology. *Earth Plan. Sci. Lett.*
431 **408**, 48–56 (2014).

432 32. Boulila, S. *et al.* Astronomical calibration of the Toarcian Stage: Implications for sequence
433 stratigraphy and duration of the early Toarcian OAE. *Earth Plan. Sci. Lett.* **386**, 98–111
434 (2014).

435 33. Peucker-Ehrenbrink, B. & Hannigan, R.E. Effect of black shale weathering on the mobility
436 of rhenium and platinum group elements. *Geology* **28**, 475–478 (2000).

437 34. Jaffe, L.A., Peucker-Ehrenbrink, B. & Petsch S.T. Mobility of rhenium, platinum group
438 elements and organic carbon during black shale weathering. *Earth Plan. Sci. Lett.* **198**, 339–
439 353 (2002).

440 35. Pierson-Wickmann, A.-C., Reisberg, L. & France-Lanord, C. Behavior of Re and Os during
441 low-temperature alteration: Results from Himalayan soils and altered black shales.
442 *Geochim. Cosmochim. Acta* **66**, 1539–1548 (2002).

443 36. Dera, G. & Donnadieu, Y. Modeling evidences for global warming, Arctic seawater
444 freshening, and sluggish ocean circulation during the Early Toarcian anoxic event.
445 *Paleoceanography* **27**, PA002283 (2012).

446 37. Georg, R.B., West, A.J., Vance, D. Newman, K. & Halliday, A.N. Is the marine osmium
447 isotope record a probe for CO₂ release from sedimentary rocks? *Earth Plan. Sci. Lett.* **367**,
448 28–38 (2013).

449 38. Tejada, M.L.G. *et al.* Ontong Java Plateau eruption as a trigger for the early Aptian oceanic
450 anoxic event. *Geology* **37**, 855–858 (2009).

451 39. Bottini, C., Cohen, A.S., Erba, E., Jenkyns, H.C. & Coe, A.L. Osmium-isotope evidence for
452 volcanism, weathering, and ocean mixing during the early Aptian OAE 1a. *Geology* **40**,
453 583–586 (2012).

454 40. Turgeon, S.C & Creaser, R.A. Cretaceous oceanic anoxic event 2 triggered by a massive
455 magmatic episode. *Nature* **454**, 323–326 (2008).

456 41. Ellam, R.M., Carlson, R.W. & Shirey, S.B. Evidence from Re-Os isotopes for plume-
457 lithosphere mixing in Karoo flood basalts genesis *Nature* **359**, 718–721 (1992).

458 42. Molzahn, M., Reisberg, L. & G. Wörner. Os, Sr, Nd, Pb, O isotope and trace element data
459 from the Ferrar flood basalts, Antarctica: evidence for an enriched subcontinental

460 lithospheric source. *Earth Plan. Sci. Lett.* **144**, 529–546 (1996).

461 43. Riley, T.R., Leat, P.T., Storey, B.C., Parkinson, I.J. & Millar, I.L. Ultramafic lamprophyres
462 of the Ferrar large igneous province: evidence for a HIMU mantle component. *Lithos* **66**,
463 63–76 (2003).

464 44. Heinonen, J.S., Carlson, R.W. & Luttinen, A.V. Isotopic (Sr, Nd, Pb, and Os) composition of
465 highly magnesian dikes os Vestfjella, western Dronning Maud Land, Antarctica: A key to
466 the origins of the Jurassic large igneous province? *Chem. Geol.* **277**, 227–244 (2010).

467 45. Heinonen, J.S., Carlson, R.W., Riley, T.R., Luttinen, A.V. & Horan, M.F. Subduction-
468 modified oceanic crust mixed with a depleted mantle reservoir in the sources of the Karoo
469 continental flood basalt province. *Earth Plan. Sci. Lett.* **394**, 229–241 (2014).

470 46. Sheldon, N.D. Abrupt chemical weathering increase across the Permian-Triassic boundary.
471 *Palaeogeo. Palaeoclim. Palaeoecol.* **231**, 315–321 (2006).

472 47. Beerling, D.J. & Berner, R.A. Biogeochemical constraints on the Triassic-Jurassic boundary
473 carbon cycle event. *Glob. Biogeo. Cycles* **16**, GB001637 (2002).

474 48. Kuroda, J., Hori, R.S., Suzuki, K., Gröcke, D.R. & Ohkouchi, N. Marine osmium isotope
475 record across the Triassic-Jurassic boundary from a Pacific pelagic site. *Geology* **38**, 1095–
476 9098 (2010).

477 49. Ravizza, G., Norris, R.N. & Blusztajn, J. An osmium isotope excursion associated with the
478 late Paleocene thermal maximum: Evidence of intensified chemical weathering.
479 *Paleoceanography* **16**, 155–163 (2001).

480 50. Hönisch, B., *et al.* The Geological Record of Ocean Acidification. *Science* **335**, 1058–1063
481 (2012).

482 51. Xu, W. *et al.* Carbon sequestration in an expanded lake system during the Toarcian oceanic

483 anoxic event. *Nature Geosci.* **10**, 129–134 (2017).

484 52. Zeebe, R.E., Ridgwell, A. & Zachos, J.C. Anthropogenic carbon release rate unprecedented
485 during the past 66 million years. *Nature* **9**, 325–329 (2016).

486 53. Parmesan, C. Ecological and Evolutionary Responses to Recent Climate Change. *Annu. Rev.*
487 *Ecol. Evol. Syst.* **37**, 637–669 (2006).

488 54. Selby, D. & Creaser, R.A. Re-Os geochronology of organic rich sediments: an evaluation of
489 organic matter analysis methods. *Chem. Geol.* **200**, 225–240 (2003).

490 55. Cumming, V.M., Poulton, S.W., Rooney, A.D. & Selby, D. Anoxia in the terrestrial
491 environment during the late Mesoproterozoic. *Geology* **41**, 583–586 (2013).

492 56. Creaser, R.A., Papanastassiou, D.A. & Wasserburg, G.J. Negative thermal ion mass
493 spectrometry of osmium, rhenium and iridium. *Geochim. Cosmochim. Acta* **55**, 397–401
494 (1991).

495 57. Völkening, J., Walczyk, T. & Heumann, K.G. Osmium isotope ratio determination by
496 negative thermal ion mass spectrometry. *Int. J. Mass Spectrom. Ion Process.* **105**, 147–159
497 (1991).

498 58. Gramlich, J.W., Murphy, T.J., Garner, E.L. & Shields, W.R. Absolute isotopic abundance
499 ratio and atomic weight of a reference sample of rhenium. *J. Res. Nat. Bur. Stds.* **77A**, 691–
500 698 (1973).

501 59. Peterson, L.C., Haug, G.H., Hughen, K.A. & Röhl, U. Rapid Changes in the Hydrologic
502 Cycle of the Tropical Atlantic During the Last Glacial. *Science* **290**, 1947–1951 (2000).

503 60. Latimer, J.C. & Filippelli, G.M. Terrigenous input and paleoproductivity in the Southern
504 Ocean. *Paleoceanography* **16**, 627–643 (2001).

505 61. Mundil, R., Ludwig, K.R., Metcalfe, I. & Renne, P.R. Age and timing of the Permian Mass

506 Extinctions: U/Pb Dating of Closed-System Zircons. *Science* **305**, 1760–1763 (2004).

507 62. Mattinson, J.M. Zircon U-Pb chemical abrasion (“CA-TIMS”) method: Combined annealing
508 and multi-step partial dissolution analysis for improved precision and accuracy of zircon
509 ages. *Chem. Geol.* **220**, 47–66 (2005).

510 63. Scoates, J.S. & Friedman, R.M. Precise age of the platiniferous Merensky Reef, Bushveld
511 Complex, South Africa, by the U-Pb zircon chemical abrasion ID-TIMS technique. *Econ.*
512 *Geol.* **103**, 465–471 (2008).

513 64. Gerstenberger, H. & Haase, G.A. Highly effective emitter substance for mass spectrometric
514 Pb isotopic ratio determinations. *Chem. Geol.* **136**, 309–312 (1997).

515 65. Thirlwall, M.F. Inter-laboratory and other errors in Pb isotope analyses investigated using a
516 207Pb - 204Pb double spike. *Chem. Geol.* **163**, 299–322 (2000).

517 66. Schmitz, M.D. & Schoene, B. Derivation of isotope ratios, errors, and error correlations for
518 U-Pb geochronology using 205Pb - 235U -(233U)-spiked isotope dilution thermal ionization
519 mass spectrometric data. *Geochem. Geophys. Geosyst.* **8**, Q08006 (2007).

520 67. Ludwig, K.R., Isoplot 3.00, A Geochronological Toolkit for Microsoft Excel. University of
521 California at Berkeley, kludwig@bge.org.

522 68. Jaffey, A.H., Flynn, K.F., Glendenin, L.E., Bentley, W.C. & Essling, A.M. Precision
523 measurement of half-lives and specific activities of 235U and 238U . *Phys. Rev.* **C4**, 1889–
524 1906 (1971).

525 69. Hall, R., McNicoll, V., Gröcke, D., Craig, J. & Johnston, K. Integrated stratigraphy of the
526 lower and middle Fernie Formation in Alberta and British Columbia, western Canada. *Riv.*
527 *Ital. Paleon. Strat.* **110**, 61–68 (2004).

528 70. Smolian, M.I., Walker, R.J. & Morgan, J.W. Re-Os ages of Group IIA, IIIA, IVA and IVB

529 iron meteorites. *Science* **271**, 1099–1102 (1996).

530 71. Scotese, C.R. *Atlas of Earth History*. PALEOMAP Project, Arlington, Texas (2001).

531

532 **Acknowledgements**

533 TRT would like to thank the Virginia Tech College of Science Roundtable grant committee for

534 the Make-a-Difference Scholarship and the ExxonMobil/Geological Society of America,

535 American Association of Petroleum Geologists, and International Association of

536 Sedimentologists graduate student grant programs for funding (IAS grant funded the pilot study).

537 A grant to BCG (EAR-1324752) and JDO (OCE-1624895) from the National Science

538 Foundation also funded this work. DS acknowledges the Total Endowment Fund. Thanks to Dr.

539 Joanna Hesselink, H. Lin, C. Wall, N. Moerhuis, and T. Ockerman for laboratory assistance, and

540 to Angela Gerhardt, Emma Tulsky, and Selva Marroquín for their help in collecting samples.

541 Sample collections were authorized by the following permits: Parks Canada, Permit No: YHTR-

542 2014-16156; RTMP, Permit No: 13-058, 14-009, 15-019. Finally, we would like to thank two

543 anonymous reviewers whose comments greatly improved the manuscript.

544

545 **Author Contributions**

546 TRT, BCG, DS, and DRG designed the study. TRT and BCG collected samples. TRT and DS

547 conducted the Re-Os geochemical analyses. JDO conducted the elemental analyses. RMF

548 conducted the U-Pb CA-ID-TIMS analyses. TRT and BCG conducted the numerical modelling.

549 All authors analysed the data. TRT and BCG wrote the paper with contributions from all the

550 authors. TRT prepared the figures.

551 **Additional Information**

552 **Competing financial interests:** The authors declare no competing financial interests.

553

554 **FIGURE CAPTIONS**

555 Figure 1. Global palaeogeography of the Early Toarcian (modified from ref. 71). Star represents
556 this study's location. Arrows point to the UK study locations^{20,23}, which are geographically close
557 to one another. Hatched outline in southern Pangaea (present-day southern Africa and
558 Antarctica) represents location and known extent of Karoo-Ferrar Large Igneous Province. Dark
559 grey represents landmasses, light blue represents shallow seas, and dark blue represents open
560 oceans. CPM = Central Pangaean Mountains. See ref. 15 for a list of locations that document the
561 T-OAE CIE.

562

563 Figure 2: Record of the osmium isotope excursion across the T-OAE CIE from Yorkshire,
564 United Kingdom²⁰ and the Mochras borehole²³. The Yorkshire dataset was originally interpreted
565 to represent a 400 – 800% increase in continental weathering rates²⁰; however, other
566 interpretations suggests that the radiogenic values during the *exaratum* ammonite subzone were
567 caused by hydrographic restriction^{21,22}. The close palaeogeographic proximity between these two
568 sites, coupled with their significantly different $^{187}\text{Os}/^{188}\text{Os}_i$ values suggests a regional influence
569 on $^{187}\text{Os}/^{188}\text{Os}_{\text{sw}}$ values in the European epicontinental seaway during the T-OAE.

570

571 Figure 3: Chemostratigraphy of the Lower Jurassic Fernie Formation from East Tributary of
572 Bighorn Creek Alberta. $\delta^{13}\text{C}_{\text{org}}$ = organic carbon isotopic compositions from ref. 15. $^{187}\text{Os}/^{188}\text{Os}_i$
573 = initial osmium isotopic composition of organic-rich sediments. Lithostratigraphic members of
574 the Fernie Formation, Stages of the Jurassic, and ammonite zonations for both northwestern

575 Europe and western North American shown to the left of the stratigraphic column (refer to ref.
576 15 for the details of their placements). Vertical gray line in $^{187}\text{Os}/^{188}\text{Os}_i$ record is the end-member
577 $^{187}\text{Os}/^{188}\text{Os}_m$ value of ~ 0.12 . We report new single zircon U-Pb CA-ID-TIMS ages of $188.58 \pm$
578 0.17 (0.25) [0.32] Ma in the bentonite at -1.9 meters and 185.49 ± 0.16 (0.25) [0.32] Ma in the
579 bentonite at 2.35 meters, located in the *margaritatus* Zone of NW Europe or the *kunae* Zone of
580 western NA (see Methods and SI Data 2).

581

582 Figure 4: Examples of the modelled osmium isotopic composition of the ocean over the T-OAE.

583 **A)** For this model run, the osmium isotopic composition of the continental input was increased to
584 2.0 and the flux of osmium from continents was increased two-fold (475.3 mol/yr) during the
585 Toarcian OAE. This resulted in the seawater osmium isotope values to increase to 0.44, which
586 does not reproduce the observed osmium isotope excursion observed at East Tributary. **B)** Model
587 run where the osmium isotopic composition and flux of the continental input of osmium was
588 increased to 2.0 by $\sim 3.4x$ respectively. This model run reproduced the osmium isotope
589 excursion. **C)** The osmium isotope composition of the continental input of osmium was kept at
590 1.4 during the Toarcian OAE, but the flux of osmium from continents was increased by $\sim 6.3x$ to
591 reproduce the osmium isotope excursion.

592

593 **Table**

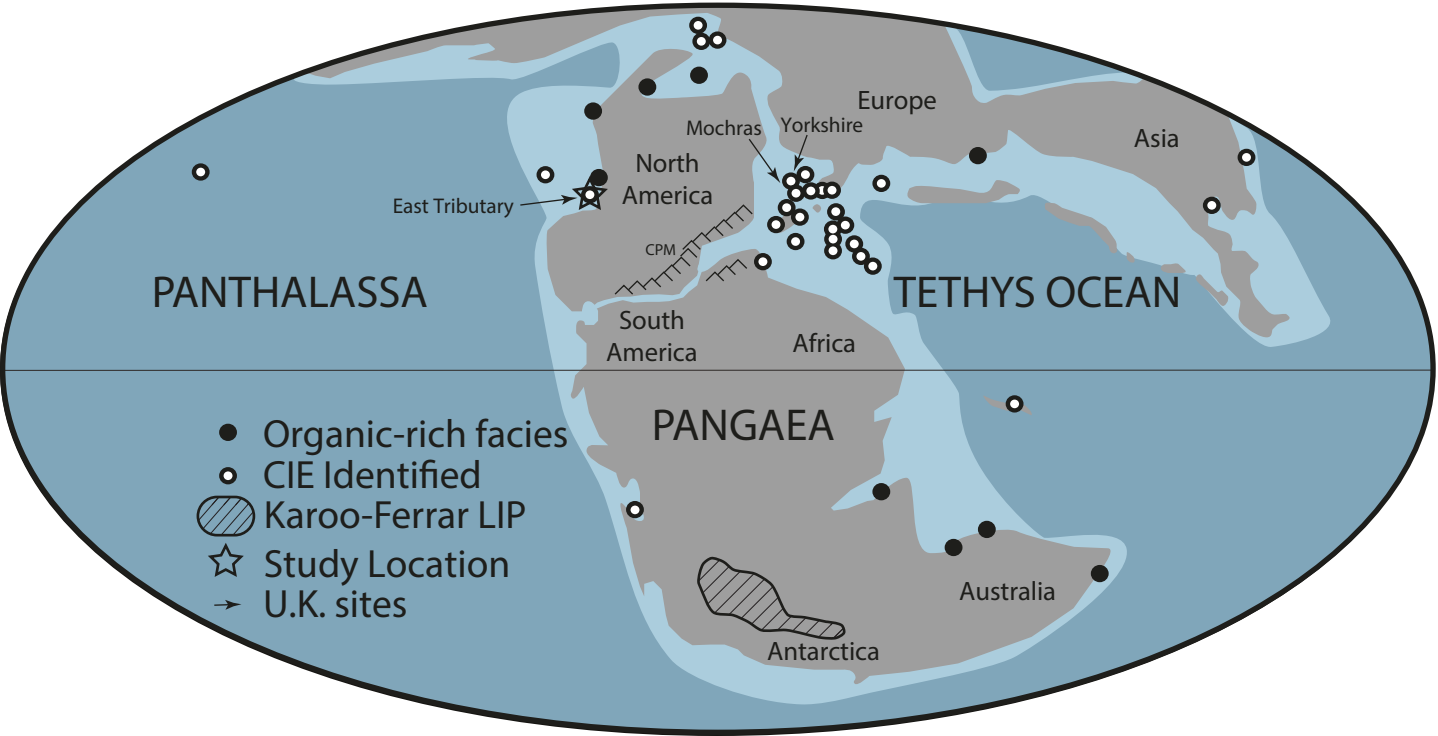
594 Table 1. Range of parameters explored modelling the osmium isotope excursion associated with
595 the Toarcian Oceanic Anoxic Event in the East Tributary and Yorkshire sections.

Model parameter	Pre- and post-T-OAE steady state	OAE state
M_{SW}^a	10^5 to 10^9	10^5 to 10^9
F_{cont}^b	238 to 524	238 to 5,500
N_{cont}	1.4 to 2.0	1.4 to 5.0
F_m^b	1,925 to 2,212	0 to 2,212
N_m	0.12	0.12
Duration ^c		300 to 500

596 ^a Reservoir unit is mol Os

597 ^b Flux units are mol/yr Os

598 ^c Duration unit is kiloyear (kyr)



PANTHALASSA

TETHYS OCEAN

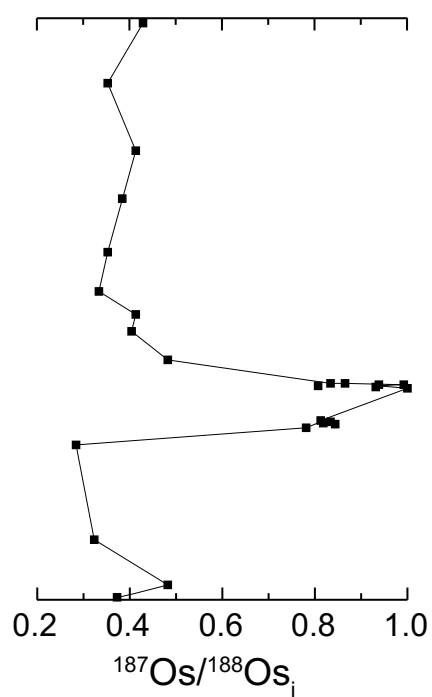
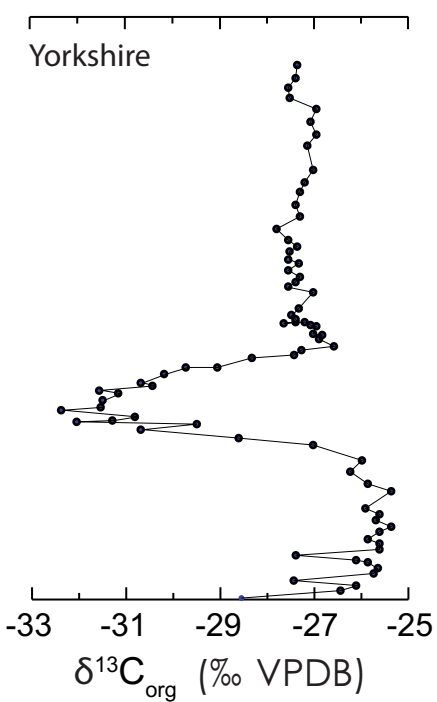
PANGAEA

- Organic-rich facies
- CIE Identified
- ▨ Karoo-Ferrar LIP
- ★ Study Location
- U.K. sites

Stage
W
North America
N.W. Europe
Mediterranean

Toarcian	planulata
	bifrons
	serpentinum
	levisoni

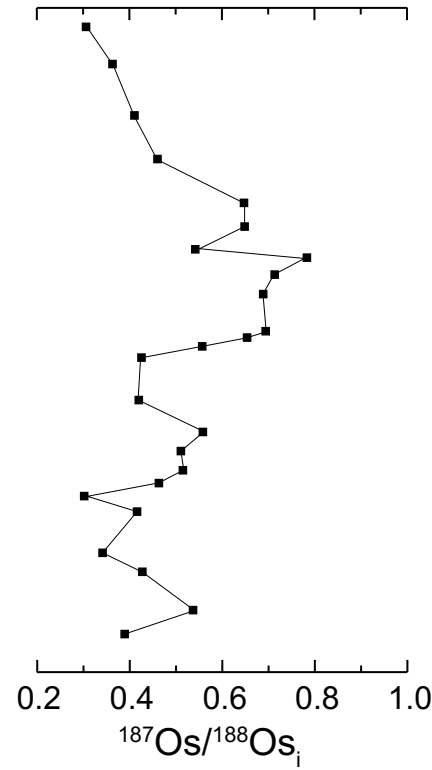
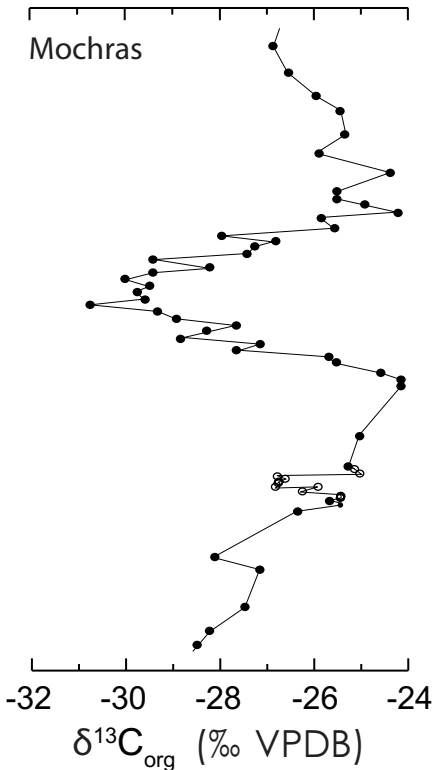
Yorkshire

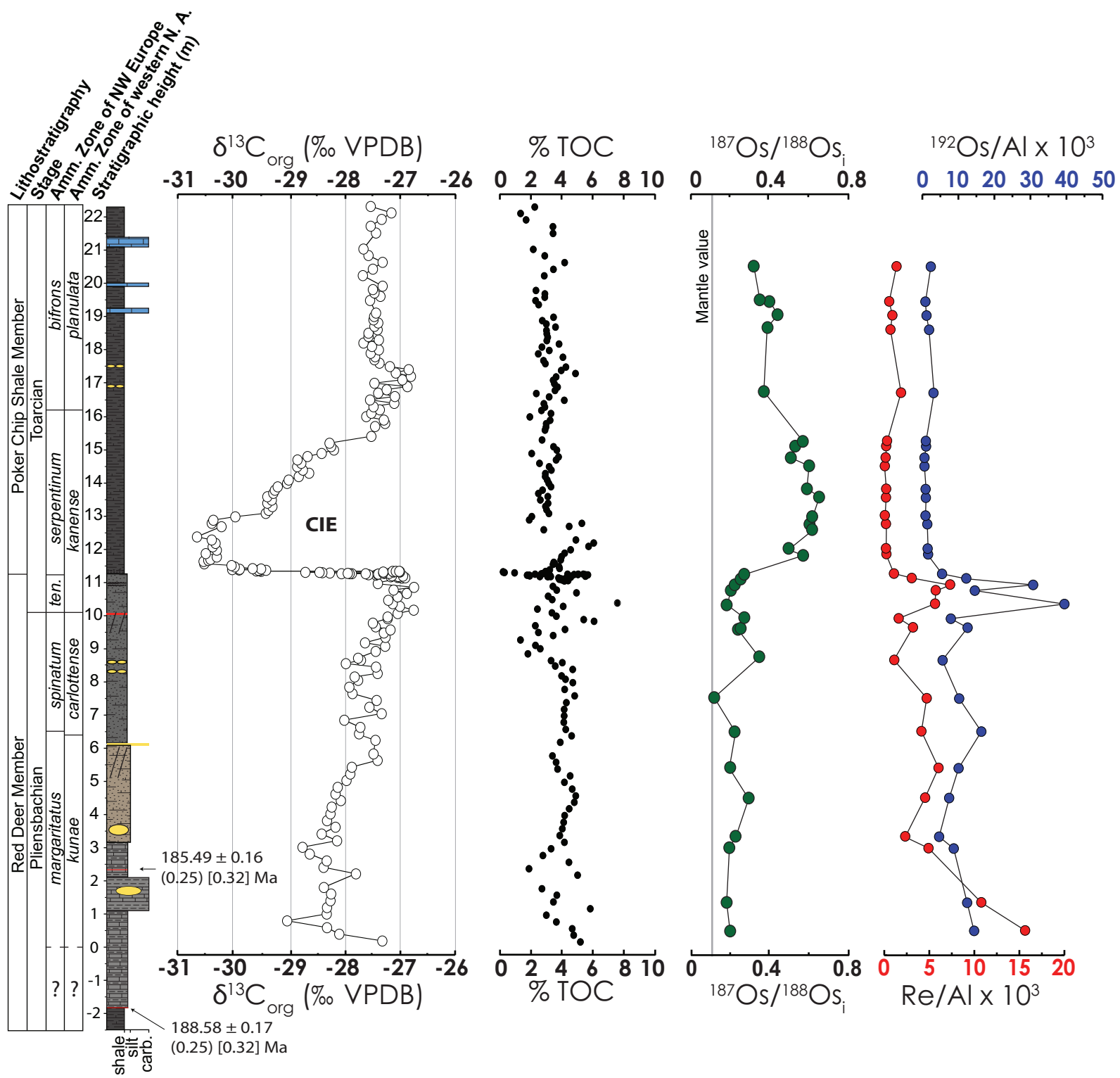


Stage
W
North America
N.W. Europe
Mediterranean

Toarcian	plan.
	bif.
	serpentinum
	levisoni

Mochras





Legend

- Calcareous mudstone
- Calcareous siltstone
- Alt. calc. mudstone/siltstone
- Unfossiliferous calc. siltstone
- Interbedded limestone w/ thin shale
- Interbedded shale/limestone
- Carbonate
- Potential hardground
- // Calcite veins
- Volcanic ash bed
- Concretions
- Sands

